# Deterministic generation of entanglement in a quantum network by coherent absorption of a single photon

Anton N. Vetlugin ®,[1,*] Ruixiang Guo,[1] Cesare Soci ®,[1,†] and Nikolay I. Zheludev ®[1,2]

[1]*Centre for Disruptive Photonic Technologies, SPMS, TPI, Nanyang Technological University, 637371 Singapore*
[2]*Optoelectronics Research Centre and Centre for Photonic Metamaterials, University of Southampton, Southampton SO17 1BJ, United Kingdom*

Advanced quantum information protocols rely on the operation of multinodal quantum networks where entanglement is distributed across the nodes. Existing protocols of entanglement generation are probabilistic, with the efficiency dropping exponentially with the size of the system. We formulate an approach for the deterministic generation of entangled states of a multinodal quantum network of arbitrary size by coupling a single photon standing wave with the nodes of the network. We show experimentally how this can be implemented in a simple binodal system. Since this approach relies on collective excitation of the network—not on local interaction with individual nodes—it allows generation of entanglement with unitary efficiency, independent of the size and the nature of the network.

## I. INTRODUCTION

Quantum technology promises to deliver powerful calculations, unbreakable secure communication, and highly sensitive measurements [1]. The key component of quantum systems is a quantum network—a system consisting of multiple nodes, able to store and process quantum information, and quantum channels connecting them [2,3]. Nodes of the quantum network are built using matter-based platforms (atoms, ions, superconducting and plasmonic systems, etc.), which may provide high precision quantum state control, long-term storage, enhanced interaction strength between quantum subsystems, and miniaturization.

To perform quantum operations, such as communication and computation, quantum entanglement should be distributed across the quantum network. For instance, entanglement can be generated in the "read-out" approach where, at the first step, entanglement between a quantum light pulse and a node of the network is generated either in the Fock [4,5] or polarization-spin [6,7] basis through the read-out process. Next, by interfering light pulses generated from two different nodes and performing detection in the maximally entangled basis [8–10], the entanglement is swapped between the corresponding nodes. In general, the read-out approaches are probabilistic and suffer from the low rate of entanglement generation. Thus, entanglement generation in multinodal networks using these schemes [11,12] is a challenging task. Another method of entanglement generation is through the "write-in" approach: a single photon coming from the external single-photon source is coherently distributed and written into the nodes of the quantum network [2,13,14]. The resulting

single-excitation entangled state of the network,

$$\sum_{m=1}^{M} b_m |0\rangle_{B_1} |0\rangle_{B_2} \cdots |1\rangle_{B_m} \cdots |0\rangle_{B_M}, \qquad (1)$$

where a single excitation is coherently distributed between $M$ nodes ($b_m$ is a probability amplitude of a single excitation to be presented in node $B_m$), forms a basis for quantum information protocols (see discussion in Sec. II E, "Quantum information with multinodal quantum networks"). To create this state, a single photon may be split into the superposition state of the multiple spatiotemporal modes on a series of beam splitters, Fig. 1(a). Each optical mode is then coupled to one of the nodes of the network *independently*. The probability of generation of state (1) in this "parallel" scheme is defined by a product of probabilities of light absorption by each node, and it decays exponentially with an increasing number of nodes: Considering a hardly achievable light-matter coupling efficiency of 90% [15] in atomic nodes, a small system composed of ten nodes will be excited in the symmetric Dicke state [$c_m = 1/\sqrt{M}$ in (1)] with a probability of $\sim 0.35$, while a network of 100 nodes will be excited in this state with a probability of $\sim 2.5 \times 10^{-5}$. The coupling efficiency in other systems, such as plasmonic structures, is significantly lower [16]. Despite these limitations, the entangled state (1) is of great interest for both fundamental research and the practical realization of quantum information protocols (see details below).

To improve the efficiency of entanglement generation in a multinodal network, we propose a "series" scheme where the entire network interacts with a single optical mode in the form of a standing wave, which drastically increases light-matter coupling efficiency. In this case, a single-photon standing wave, interacting with an array of *weakly absorbing* nodes, Fig. 1(b), may be coupled to the system deterministically:
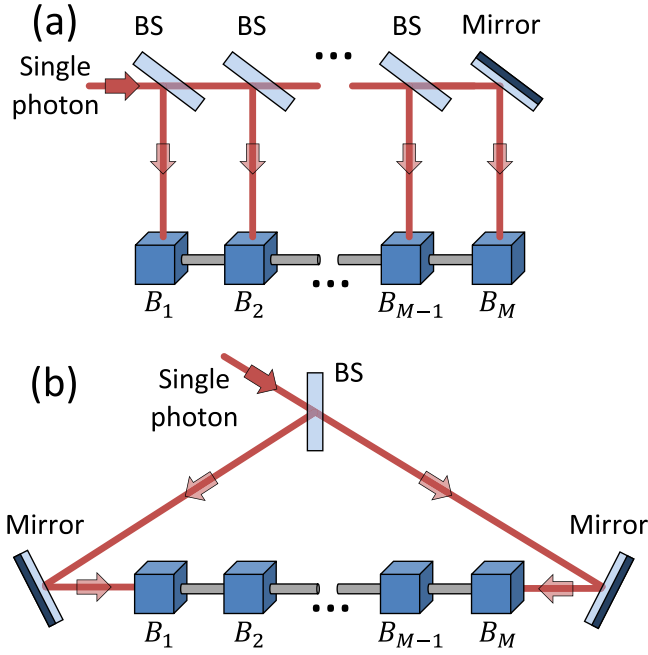
*a.vetlugin@ntu.edu.sg
†csoci@ntu.edu.sg

FIG. 1. Generation of nonclassical states of multinodal network by single-photon coupling. (a) Parallel scheme: photon is split on a series of beam splitters (BSs) and each "part" of the photon is independently coupled to corresponding nodes $B_1, \ldots, B_M$ of the network. (b) Series scheme: photon is converted into a standing wave in the interferometer configuration and coherently coupled to the multinodal network.
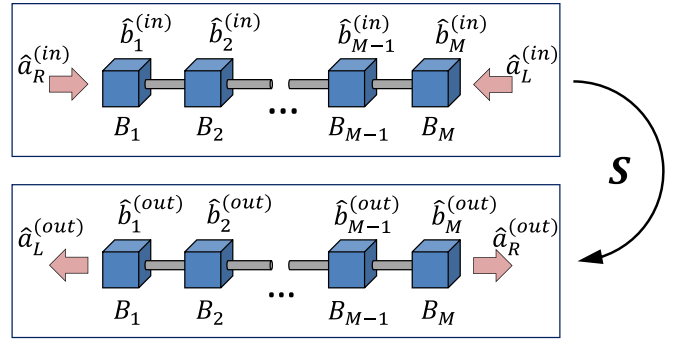


FIG. 2. Model of quantum light and multinodal network interaction. At initial time, system is described by amplitudes $\hat{a}_R^{(\mathrm{in})}$ and $\hat{a}_L^{(\mathrm{in})}$ of two coherent light modes propagating in opposite directions and carrying a single excitation and by input amplitudes $\hat{b}_m^{(\mathrm{in})}$ of the corresponding nodes in a vacuum state. At final time, system is characterized by two outgoing light modes, $\hat{a}_R^{(\mathrm{out})}$ and $\hat{a}_L^{(\mathrm{out})}$, and output amplitudes $\hat{b}_m^{(\mathrm{out})}$ of the nodes. The transformation is described by the scattering matrix $S$.

while individual nodes absorb light probabilistically, under certain conditions they may act together as an *ideal* coherent absorber. Based on this analysis, we fabricate a binodal system consisting of remote metallic layers of nanometer thickness that possess the required optical response and demonstrate absorption of heralded single photons by the structure with efficiency close to 90%, as opposed to the expected 20% for the parallel scheme. Assuming unitary light-matter exchange interaction, we show that the photon is absorbed nonlocally and the multinodal quantum network is excited into an entangled quantum state (1).

## II. RESULTS

### A. Coupling of a single-photon standing wave into a multinodal quantum network (theory)

We consider a quantum network (QN) consisting of $M$ nodes (quantum network nodes, QNNs), Fig. 2. The nodes could comprise any absorbing system, such as atoms, ions, quantum dots, color centers, and plasmonic or polaritonic systems. A single photon to be coupled to the QN propagates in the interferometer, where it is converted into a superposition of the left $|1\rangle_L|0\rangle_R$ and right $|0\rangle_L|1\rangle_R$ propagating photons with a controllable phase delay $\varphi$,

$$\frac{1}{\sqrt{2}}(|1\rangle_L|0\rangle_R - e^{i\varphi}|0\rangle_L|1\rangle_R). \tag{2}$$

The unitary evolution of the light-QN system can be described as

$$\begin{pmatrix} \hat{a}_L^{(\mathrm{out})} \\ \hat{a}_R^{(\mathrm{out})} \\ \hat{b}_1^{(\mathrm{out})} \\ \vdots \\ \hat{b}_M^{(\mathrm{out})} \end{pmatrix} = S \begin{pmatrix} \hat{a}_L^{(\mathrm{in})} \\ \hat{a}_R^{(\mathrm{in})} \\ \hat{b}_1^{(\mathrm{in})} \\ \vdots \\ \hat{b}_M^{(\mathrm{in})} \end{pmatrix}. \tag{3}$$

Here $\hat{a}_L(\hat{a}_R)$ are the amplitudes of the light modes propagating to the left (right) (Fig. 2) and $\hat{b}_m$ is the bosonic amplitude of the $m$th QNN. The upper index defines the amplitudes before "(in)" and after "(out)" interaction. Matrix $S$ is a square unitary matrix with components $S_{ij}$ ($i, j = 1, 2, \ldots, M + 2$) where the components $S_{11}$ and $S_{22}$ ($S_{12}$ and $S_{21}$) represent the total amplitude transmission (reflection) coefficients of the network defined under a single side illumination. Under the reciprocity principle, we set $S_{11} = S_{22} \equiv t$ and we assume $S_{12} = S_{21} \equiv r$. Practically, the unitarity of the evolution (3) means that the light temporal modes are much shorter than the characteristic decay time of the QNNs' excitations. We note that some protocols of quantum information, such as quantum key distribution, do not require storage of quantum information in the QNNs for a long time [3], and unitarity is a valid assumption for these protocols. We emphasize that the $S$ matrix differs from the scattering matrix discussed in the literature on coherent absorption of quantum light. For instance, in [17–20] the source of absorption was dissipation, and only the dynamics of light was considered. As a result, the scattering matrix was nonunitary. Here, we include the absorbing nodes of the QN into consideration; that is, excitations do not leave the entire system preserving unitarity of the $S$ matrix.

In the middle of the interferometer, the symmetric state excites a standing wave [17] with a $\cos kz$ spatial profile, $\frac{1}{\sqrt{2}}(|1\rangle_L|0\rangle_R + |0\rangle_L|1\rangle_R) \to |1\rangle_{\cos}$, while the antisymmetric

state excites a standing wave with a $\sin kz$ spatial profile, $\frac{1}{\sqrt{2}}(|1\rangle_L|0\rangle_R - |0\rangle_L|1\rangle_R) \to |1\rangle_{\text{sin}}$. As shown in Appendix A, the deterministic coupling of a single photon into the QN, that is,

$$\langle \hat{a}_L^{(\text{out})\dagger} \hat{a}_L^{(\text{out})} \rangle = \langle \hat{a}_R^{(\text{out})\dagger} \hat{a}_R^{(\text{out})} \rangle = 0,$$

can be achieved under the following two conditions: (1) QNNs are placed at antinodes of the standing wave (cosine or sine) excited by the input single photon, and (2) the amplitude transmission $t$ and reflection $r$ coefficients of the entire network are equal and in phase (for the cosine wave) or out of phase (for the sine wave): $r = \pm t$. For the general input state (2) and $r = +t$ the photon can be found on the left side or the right side of the QN with an equal probability:

$$\langle \hat{a}_L^{(\text{out})\dagger} \hat{a}_L^{(\text{out})} \rangle = \langle \hat{a}_R^{(\text{out})\dagger} \hat{a}_R^{(\text{out})} \rangle = |t|^2 (1 - \cos\varphi). \quad (4)$$

In the extreme case of $r = \pm t = -1/2$, the photon coupling efficiency $(1 - \langle \hat{a}_L^{(\text{out})\dagger} \hat{a}_L^{(\text{out})} \rangle - \langle \hat{a}_R^{(\text{out})\dagger} \hat{a}_R^{(\text{out})} \rangle)$ varies between 0 and 1, allowing to couple in or transmit the photon on demand for in-line operation and feed-forward protocols. Full transmission occurs when the QNNs are placed at the *nodes of the standing wave* where, assuming subwavelength dimensions, they do not interact with the electric field (see Appendix B).

## B. Building a multinodal network for efficient photon coupling

The components of the scattering matrix $\boldsymbol{S}$ will depend on the particular realization of the QN and the type of light-QNN interaction. As we have shown, even without knowledge of the entire $\boldsymbol{S}$ matrix, we still may achieve perfect single-photon coupling just defining the total transmission and total reflection coefficients of the entire QN, or $S_{11}$, $S_{12}$, $S_{21}$, and $S_{22}$ components of the $\boldsymbol{S}$ matrix. Moreover, from a practical point of view, all we need to know is the optical response of individual QNNs. For instance, for the basic binodal network consisting of subwavelength plasmonic structures, transmission ($t_1$ and $t_2$) and reflection ($r_1$ and $r_2$) coefficients of individual nodes are linked as (see Appendix B)

$$r_1 = t_1 - 1, \quad r_2 = t_2 - 1, \quad t_2 = \frac{t_1}{3t_1 - 1}, \quad (5)$$

where the first two equations are fulfilled automatically [18] and the last one matches transmission coefficients of the nodes. Here $t_1$ is considered as a free parameter. If placed at the antinodes of the standing wave, the QNNs (5) guarantee the total QN response of $r = +t = -1/2$. For a multicomponent system with $M > 2$, relations similar to (5) become more complicated with a number of free parameters. The solution can be simplified for the important case of $M$ identical nodes:

$$t_m = \frac{M}{M+1}, \quad r_m = t_m - 1 = -\frac{1}{M+1},$$
$$a_m^2 \equiv 1 - t_m^2 - r_m^2 = \frac{2M}{(M+1)^2}, \quad (6)$$

where $t_m$ and $r_m$ are the amplitude transmission and reflection coefficients of the $m$th node, and $a_m^2$ defines the intensity absorption coefficient (or probability of photon absorption) of each node. For instance, the total transmission and reflection

coefficients of the QN consisting of 100 nodes with transmission and reflection coefficients of $100/101$ and $-1/101$, respectively, spaced by an integer number of $\lambda$, equal to $-1/2$. Such a network will absorb a single-photon standing wave deterministically despite the fact that the intensity absorption coefficient of each node is less than 2%. Similar analysis of the optical response of the QNNs can be done for nodes of different nature in order to ensure absorption of a single-photon standing wave.

### C. Coupling of a single-photon standing wave into a binodal system (experiment)

As a proof of principle, we experimentally demonstrated efficient coupling of a single-photon standing wave in an elementary binodal system represented by ultrathin metallic layers. Two chromium layers were deposited on opposite sides of a transparent substrate (SiN) by thermal evaporation. The thickness of the chromium layers was adjusted around the nominal value of 5 nm to obtain transmission of $t_1 \approx 2/3$ and reflection of $r_1 \approx -1/3$ and $a_m^2 \approx 4/9$ in accordance with (6). The thickness of the substrate, $D_{\text{sub}} = 200$ nm, was chosen to be $\sim \lambda/2n_{\text{sub}}$ at 810 nm (based on the refractive index $n_{\text{sub}} \approx 2.02$) so that the two chromium layers could be placed at neighboring nodes of the standing wave. The optical response of such sample fulfills the condition of $r = t = -1/2$.

Degenerate spontaneous parametric down-conversion in a BBO crystal, induced by a 405 nm laser, was used to generate pairs of time-correlated signal and idler photons at the wavelength of 810 nm, Fig. 3(a). Detection of the idler photon by a single-photon avalanche photodiode SPAD-h heralds the presence of the correlated signal photon. The signal photon was prepared in the state (2) by sending it through a 50:50 beam splitter and repeatedly varying the interferometer phase $\varphi$ by a fiber stretcher. The fiber stretcher was controlled by a ramp voltage at 1 Hz modulation frequency and amplitude $9\,V_{\text{pp}}$, which ensured fiber length modulation greater than $2\lambda$ in every cycle. The coherence length of the heralded photons ($\sim 100\,\mu$m) was much greater than $D_{\text{sub}}$. Beam splitters were used to direct the outgoing photons to SPAD-1 and SPAD-2. Coincidence counts between detectors SPAD-1 and SPAD-h ($N_1$) and SPAD-2 and SPAD-h ($N_2$) were measured by a time-to-digital converter ID800 (IDQ) as a function of the phase $\varphi$. Acquisition time was set to 20 ms and data were averaged over more than 50 phase cycles. To evaluate the probability of single-photon detection by SPAD-1 ($P_1$) and SPAD-2 ($P_2$), we used the average total input photon flux as a reference:

$$P_{1,2}(\varphi) = \frac{N_{1,2}(\varphi)[\text{with absorber}]}{N_1[\text{without absorber}] + N_2[\text{without absorber}]}.$$

The slow operation rate of the detectors and relatively low coincidence count rates did not allow us to perform measurements faster than the characteristic time of the phase noise (thermal and mechanical noise of the interferometer, which has a bandwidth of $\sim 1$ Hz). To implement averaging of subsequent phase cycles, a reference-based postselection technique was used [19].

The measured single-channel probabilities $P_1(\varphi)$ and $P_2(\varphi)$ are shown by blue circles and red diamonds in Fig. 3(b). Both probabilities are in good agreement with the expected
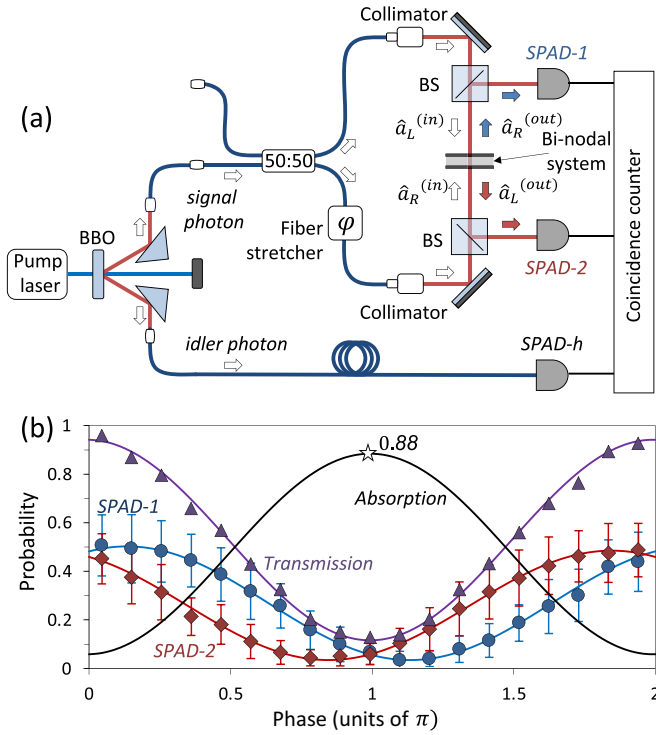
FIG. 3. Coherent absorption of heralded single photons by a binodal system. (a) Schematic of the setup with a binodal absorber placed in the middle of the interferometer. Dark blue lines correspond to the optical fiber and red lines to the free space paths of the photons. (b) Measured probabilities of heralded signal photon detection by SPAD-1 (blue circles and fitting line) and SPAD-2 (red diamonds and fitting line), total transmission (purple triangles and fitting line), and total coupling (black line) probabilities as a function of phase delay $\varphi$ between the two arms of the interferometer. The error bars represent the Poisson noise of randomly arriving photons. The highest photon absorption probability of 0.88 is marked by the white star.

behavior (4) and the corresponding fitting curves exhibit visibilities of 87%. The probabilities $P_1(\varphi)$ and $P_2(\varphi)$ oscillate almost in phase with a small shift of less than $0.3\pi$. This shift is attributed to slight discrepancies between nominal and effective optical path length of the silicon nitride membrane: Spectral measurement of the bare membrane of nominal thickness 200 nm revealed a transmission peak at 861 nm, which corresponds to an optical path length of $\approx 431$ nm rather than its nominal value of $n_{\text{sub}}D_{\text{sub}} = 2.02 \times 200$ nm $= 404$ nm. Visibility of the total transmission probability, $P_1(\varphi) + P_2(\varphi)$, shown by the purple triangles and the fitting line is around 78%, demonstrating high contrast modulation between the regimes of coherent transmission and coherent coupling of the photon. The probability, $1 - P_1(\varphi) - P_2(\varphi)$, of a single photon coupling to the structure is shown by the black line in Fig. 3(b). The maximum achieved probability of single-photon coupling was 88% [shown by the white star in Fig. 3(b)]. This probability far exceeds the maximum probability of a single-photon coupling in a conventional parallel scheme. In the latter case, coupling efficiency to each node, $1 - |t_1|^2 - |r_1|^2$, equals 4/9, assuming total coupling efficiency into two nodes of 20%.

The advantage of coherent illumination becomes even more pronounced with the increase of the number of QNNs: The coupling efficiency does not change under coherent illumination and may still reach 100% for high-dimensional systems, while it decays exponentially with the nodes number increased for parallel scheme. Note that the "series" approach has no limitations on the number of nodes constituting the quantum network. Moreover, the higher the node number, the weaker coupling of light to a single QNN is required. We emphasize that collective interaction of QNNs with a single photon allows achieving deterministic photon absorption without optical cavities [21,22].

### D. Quantum state of a multinodal network (theory)

Coupling of a single-photon standing wave into the QN could result in deterministic generation of entanglement if nodes maintaining quantum coherence (e.g., atoms, ions, plasmons, etc.) are used. Here, we assume that light coupling into QNNs happens due to a light-matter exchange interaction of the form $\hat{b}^\dagger\hat{a}$, where annihilation of a light quantum followed by excitation of a node quantum. To retrieve the quantum state of the system after photon coupling, we use the reverse to (3) transformation:

$$\begin{pmatrix} \hat{a}_L^{(\text{in})} \\ \hat{a}_R^{(\text{in})} \\ \hat{b}_1^{(\text{in})} \\ \vdots \\ \hat{b}_M^{(\text{in})} \end{pmatrix} = S^\dagger \begin{pmatrix} \hat{a}_L^{(\text{out})} \\ \hat{a}_R^{(\text{out})} \\ \hat{b}_1^{(\text{out})} \\ \vdots \\ \hat{b}_M^{(\text{out})} \end{pmatrix}.$$

By substituting the matrix components $S_{11} = S_{22} = \pm S_{12} = \pm S_{21} = t$, defined above, we find

$$\hat{a}_L^{(\text{in})} = t^*\left(\hat{a}_L^{(\text{out})} \pm \hat{a}_R^{(\text{out})}\right) + \sum_{m=1}^{M} S^*_{(m+2)1}\hat{b}_m^{(\text{out})},$$

$$\hat{a}_R^{(\text{in})} = t^*\left(\pm\hat{a}_L^{(\text{out})} + \hat{a}_R^{(\text{out})}\right) + \sum_{m=1}^{M} S^*_{(m+2)2}\hat{b}_m^{(\text{out})}.$$

Now, for instance, for $S_{11} = S_{22} = S_{12} = S_{21} = t$, the sine standing wave carrying a single photon,

$$|1\rangle_{\text{sin}} \leftarrow \frac{1}{\sqrt{2}}(|1\rangle_L|0\rangle_R - |0\rangle_L|1\rangle_R) = \frac{1}{\sqrt{2}}\left(\hat{a}_L^{(\text{in})\dagger} - \hat{a}_R^{(\text{in})\dagger}\right)|\text{vac}\rangle,$$

is transformed into the output superposition state of the multinodal QN of the form

$$\frac{1}{\sqrt{2}} \sum_{m=1}^{M} (S_{(m+2)1} - S_{(m+2)2})\hat{b}_m^{(\text{out})\dagger}|\text{vac}\rangle$$

$$= \frac{1}{\sqrt{2}} \sum_{m=1}^{M} (S_{(m+2)1} - S_{(m+2)2})|0\rangle_{B_1}|0\rangle_{B_2}\cdots|1\rangle_{B_m}\cdots|0\rangle_{B_M}.$$

$$(7)$$

State (7) is exactly the state of interest (1), where $b_m = (S_{(m+2)1} - S_{(m+2)2})/\sqrt{2}$. This state ensures that the single

photon is distributed coherently among spatially separated nodes. Similarly, it can be shown that for $S_{11} = S_{22} = -S_{12} = -S_{21} = t$, the cosine standing wave carrying a single photon will be coupled to the network creating a state similar to (7). The probability amplitude of photon absorption by the $m$th node is defined by the corresponding elements of the first two columns of the $S$ matrix which, in turn, depend on the coupling strength between light and the node. To change the resulting quantum state of the system it is sufficient to change the optical response of individual nodes while keeping the total system response constant. Since the wave function (7) is normalized, the larger the network the smaller the absolute values of the $S$-matrix components may be and, correspondingly, the smaller coupling efficiency between light and individual nodes is required. As a result, quantum light may be perfectly coupled to an array of weakly absorbing nodes exciting the QN entangled state.

### E. Quantum information with multinodal quantum networks

As practical applications require multiparticle entanglement, the use of a single-particle entangled state (1) is somewhat limited. Nevertheless, as shown in the following, it is possible to obtain a system with multiparticle entanglement by stacking subsystems carrying the state (1). As an example, we consider a scheme suitable for multiparty quantum cryptography, or Bell inequality detection, Fig. 4(a). The scheme can be considered as an extension of the corresponding two-party Duan-Lukin-Cirac-Zoller (DLCZ) scheme [23]. The whole network consists of two subsystems, $B$ and $C$, each prepared in a symmetric state of the form of Eq. (1): $\frac{1}{\sqrt{M}}(\hat{b}_1^\dagger + \hat{b}_2^\dagger + \cdots + \hat{b}_M^\dagger)|\text{vac}\rangle$ and $\frac{1}{\sqrt{M}}(\hat{c}_1^\dagger + \hat{c}_2^\dagger + \cdots + \hat{c}_M^\dagger)|\text{vac}\rangle$, respectively, where $|\text{vac}\rangle$ stands for the vacuum state of the network. Each party holds one node of each subsystem: Party 1 (Alice) holds (conjugate) nodes $B_1$ and $C_1$, party 2 (Bob) holds $B_2$ and $C_2$, party 3 (Charlie) holds $B_3$ and $C_3$, and so on as shown by dashed boxes in Fig. 4(a). Next, each party reads the state of the conjugate nodes as shown in Fig. 4(a), where the detector $D_{m\pm}$ performs measurement of $\hat{D}_{m\pm}^\dagger \hat{D}_{m\pm}$ with $\hat{D}_{m\pm} = (\hat{b}_m \pm \hat{c}_m)/\sqrt{2}$. The coincidence between counts of the detectors belonging to different parties will be registered with probability $1 - 1/M$, and we are interested in these events. For instance, the coincidence between Alice's and Bob's detectors reduces the network wave function to $\frac{1}{\sqrt{2}}(\hat{b}_1^\dagger \hat{c}_2^\dagger + \hat{b}_2^\dagger \hat{c}_1^\dagger)|\text{vac}\rangle$, or $\frac{1}{\sqrt{2}}(\hat{D}_{1+}^\dagger \hat{D}_{2+}^\dagger - \hat{D}_{1-}^\dagger \hat{D}_{2-}^\dagger)|\text{vac}\rangle$, where detectors' counts of different parties are correlated. From this point on, the protocols will be exactly equivalent to the two-party DLCZ scheme. For instance, to generate a common key, each party applies a phase shift $\varphi_m$, chosen randomly from the basis $\{0, \pi/2\}$, to one of the optical paths, Fig. 4(a). If the applied phase shifts coincide, the whole wave function just acquires a common phase, and correlations are preserved. If the phase shifts are opposite, the state changes to $\frac{1}{\sqrt{2}}(\hat{b}_1^\dagger \hat{c}_2^\dagger - \hat{b}_2^\dagger \hat{c}_1^\dagger)|\text{vac}\rangle$, or $\frac{1}{\sqrt{2}}(\hat{D}_{1+}^\dagger \hat{D}_{2-}^\dagger - \hat{D}_{1-}^\dagger \hat{D}_{2+}^\dagger)|\text{vac}\rangle$, where the correlation between detectors' counts is changed. Since the applied phase shifts are later shared using an open communication channel, the parties
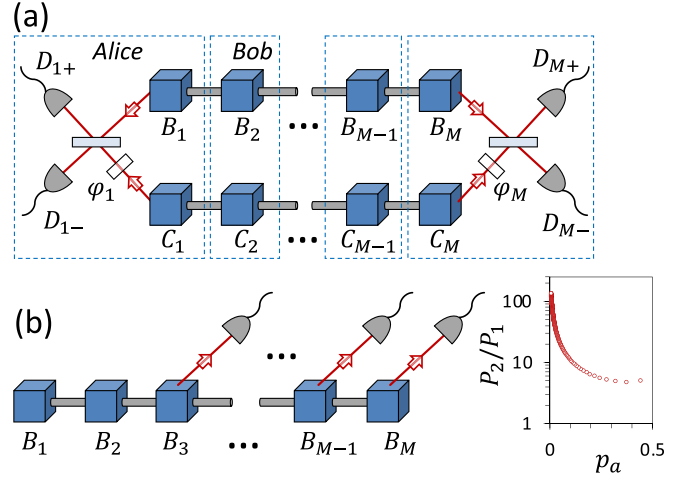


FIG. 4. Quantum information protocols with entangled multinodal networks. (a) Multiparty quantum key distribution. Two subsystems, $B$ and $C$, compose the network, where the $m$th party holds one node of each subsystem, $B_m$ and $C_m$ ($m = 1, 2, \ldots, M$). The protocol starts with coherent distribution of a single photon in each subsystem, so that two excitations are present in the whole network. Next, each party performs measurement of conjugated nodes $B_m$ and $C_m$ by transferring their states to light modes, applying the phase shift $\varphi_m$ (randomly chosen either 0 or $\pi$) to one of them, and mixing them on a beam splitter [for simplicity, measurement setups are shown only for the first (Alice) and last parties]. Quantum key distribution is based on correlation measurement between detectors' counts belonging to different parties. (b) Efficient excitation of entangled states of a system composed of two weakly absorbing nodes. First, a single photon is deterministically coupled to a multinodal network of a higher dimension creating its entangled state. By measuring the state of nodes $B_3$, $B_4$, $\ldots$, $B_M$, the wave function is reduced to the entangled state of two nodes $B_1$ and $B_2$. Ratio $P_2/P_1$ of probabilities of entanglement generation for the series scheme ($P_2$) compared to the parallel scheme ($P_1$) is shown in the graph as a function of the photon coupling probability $p_a$ in each node.

know the type of correlations between the detector counts, and these trials are used to generate a common key. The rate of key generation between different parties in the network can be altered by changing the coefficients in the initial states of the subsystems $B$ and $C$. Similarly, other quantum information protocols can be realized; for instance, quantum teleportation can be implemented either in a similar probabilistic one-to-one way or from one party to the collective state of the rest of the network, where the teleported state is coherently distributed between parties. More sophisticated protocols can also be implemented by adding more subsystems, and cluster (graph) states [24,25] and quantum circuit architectures [26] could possibly benefit from using this approach.

Multinodal networks can be also used to speed up the preparation of quantum states of smaller networks. Let us consider the case in which the entangled state,

$$\frac{1}{\sqrt{2}}(|1\rangle_{B_1}|0\rangle_{B_2} + |0\rangle_{B_1}|1\rangle_{B_2}), \tag{8}$$

between nodes $B_1$ and $B_2$ is created using a single-photon source and weakly absorbing samples. The probability of

photon absorption $p_a$ by each node is less or significantly less than 1. In the parallel scheme based on splitting of the photon and coupling light to each node, Fig. 1(a), the required state is created with probability $P_1 = p_a^2$. This probability can be increased by using the series scheme, Fig. 1(b). First, a single photon is coherently coupled to a system composed of $M$ weakly absorbing nodes generating the state (1) with $b_m = 1/\sqrt{M}$. The number of nodes $M$ is chosen so that the photon is coupled deterministically to the system despite the low photon absorption probability $p_a$ in each node. Next, the state of the $M$th node is read out, where with probability $1-1/M$ (for ideal detectors) no excitation is detected with the following projection of the state of the rest of the network to

$$\frac{1}{\sqrt{M-1}} \sum_{m=1}^{M} |0\rangle_{B_1} |0\rangle_{B_2} \cdots |1\rangle_{B_m} \cdots |0\rangle_{B_{M-1}}.$$

By repeating this procedure $M-2$ times (for nodes $M-1$, $M-2$, ..., 3), the state of the system is reduced to (8) with overall success probability $P_2 = 2/M$ (all $M-2$ nodes can be read out simultaneously). The ratio $P_2/P_1$ as a function of a single-node absorption probability $p_a$ is shown in the graph in Fig. 4(b), where $p_a$ is set as $2M/(M+1)^2$ [$p_a = a_m^2$ from Eq. (6)]. The speed-up advantage of using the series scheme is clearly seen in the graph.

The quantum information protocols discussed here could be used to experimentally verify the excitation of state (1) or (7). These experiments would require manipulation of the atomic ensembles [13,14], plasmons [16,27], phonons [28], or other systems where absorbed excitation of a single photon can be stored and reversed back to the optical fields for further detection.

## III. DISCUSSION

We demonstrated theoretically that the quantum regime of deterministic coherent single-photon absorption may be achieved in multinodal quantum networks. As a proof-of-principle demonstration, we conducted an experiment where single photons are absorbed in a binodal system with efficiency close to unity. While the existing approaches do not allow efficient generation of entanglement in multinodal QNs, the efficiency of the approach developed here is independent of the number of nodes constituting the network. Remarkably, requirements on the coupling of light to each node of the network are loosened in larger networks for the standing wave excitation, allowing one to deterministically absorb photons in QNs composed of weakly absorbing nodes. To exploit the advantage of the standing wave coupling, the physical dimension of the network (the distance between the first and the last nodes of the network) should be within the coherence length of a single photon. Therefore, the proposed method can be directly applied using a narrowband single-photon source [29] or in miniaturized (integrated) quantum networks [30,31], while quantum repeater protocols [32] may be necessary to swap entanglement between remote multinodal coherent networks.

As we have shown, efficient coupling of a single-photon standing wave generates entangled states of the multinodal

QN assuming unitary light-matter exchange interaction in the nodes of the network. The resulting quantum state, where single excitation is coherently spread between spatially separated QNNs, may be controlled by adjusting the optical parameters of the network components while keeping the overall optical response of the network constant. Despite being useful for the generation of entanglement in quantum networks, the approach developed here may also be applied to the protocols of quantum memory [33–36] and to excitation of quantum states of periodic systems such as arrays of atoms [37,38] and ions [39,40], which are promising platforms for quantum computation [41–43] and quantum simulations [44,45] as well as for the study of the fundamental effects [28,46]. Also, periodic structures may be used for coherent schemes [47] of classical [48–51] and quantum [18,52–61] light manipulation in free space and in integrated platforms [19,62–64].

In conclusion, multinodal quantum networks are the foundation of quantum information protocols, including quantum computation and quantum communication, and the ability to manipulate quantum states of such networks is a necessary requirement for the development of quantum technology. Single-photon standing wave coupling discussed here provides a robust and efficient way to generate and control quantum entanglement in multinodal quantum networks.

The data that supports the findings of this study are openly available in NTU research data repository DR-NTU (Data) at [65].

## APPENDIX A: GENERAL MODEL OF DETERMINISTIC COUPLING OF A SINGLE PHOTON TO MULTINODAL QUANTUM NETWORK

In this Appendix, we derive the conditions for deterministic coupling of a single photon to a multinodal quantum network based on the model shown in Fig. 2 of the main text. We consider two counterpropagating coherent light modes with quantized amplitudes $\hat{a}_L^{(in)}$ and $\hat{a}_R^{(in)}$ which illuminate a medium consisting of $M$ spatially separated nodes. The size of the whole structure is supposed to be much smaller than the coherence length of light. For the $m$th node, we define a bosonic amplitude $\hat{b}_m^{(in)}$ and initial vacuum state $|0\rangle_{B_m}$. After

the interaction, the system is characterized by the output light ($\hat{a}_L^{(out)}$ and $\hat{a}_R^{(out)}$) and node ($\hat{b}_m^{(out)}$) amplitudes, where a linear transformation is described by the $S$ matrix with components $\{S_{ij}\}$ ($i, j = 1, 2, \ldots, M + 2$):

$$
\begin{pmatrix}
\hat{a}_1^{(out)} \\
\hat{a}_2^{(out)} \\
\hat{b}_1^{(out)} \\
\vdots \\
\hat{b}_M^{(out)}
\end{pmatrix}
= S
\begin{pmatrix}
\hat{a}_1^{(in)} \\
\hat{a}_2^{(in)} \\
\hat{b}_1^{(in)} \\
\vdots \\
\hat{b}_M^{(in)}
\end{pmatrix}
+
\begin{pmatrix}
\hat{f}_{a1} \\
\hat{f}_{a2} \\
\hat{f}_{b1} \\
\vdots \\
\hat{f}_{bM}
\end{pmatrix}.
\tag{A1}
$$

For generality, we also include here a column vector containing Langevin noise operators $\hat{f}$. This column is responsible for the conservation of commutation relations in the presence of dissipation processes (such as the decay of the excited states of the nodes). Standard boson commutation relations are valid for light and media amplitudes: For instance, $[\hat{a}_L^{(in)}, \hat{a}_L^{(in)\dagger}] = [\hat{b}_m^{(in)}, \hat{b}_m^{(in)\dagger}] = [\hat{a}_L^{(out)}, \hat{a}_L^{(out)\dagger}] = [\hat{b}_m^{(out)}, \hat{b}_m^{(out)\dagger}] = 1$ and $[\hat{a}_L^{(in)}, \hat{a}_R^{(in)\dagger}] = [\hat{a}_L^{(in)}, \hat{b}_m^{(in)\dagger}] = [\hat{b}_m^{(out)}, \hat{b}_n^{(out)\dagger}]_{m \neq n} = 0$ and so on. Deterministic absorption of the input light requires no excitation in the outgoing light modes,

$$
\langle \hat{a}_L^{(out)\dagger} \hat{a}_L^{(out)} \rangle = \langle \hat{a}_R^{(out)\dagger} \hat{a}_R^{(out)} \rangle = 0,
\tag{A2}
$$

where, accounting for transformation (A1),

$$
\begin{aligned}
\langle \hat{a}_L^{(out)\dagger} \hat{a}_L^{(out)} \rangle &= |S_{11}|^2 \langle \hat{a}_L^{(in)\dagger} \hat{a}_L^{(in)} \rangle + |S_{12}|^2 \langle \hat{a}_R^{(in)\dagger} \hat{a}_R^{(in)} \rangle \\
&\quad + S_{11}^* S_{12} \langle \hat{a}_L^{(in)\dagger} \hat{a}_R^{(in)} \rangle \\
&\quad + S_{11} S_{12}^* \langle \hat{a}_R^{(in)\dagger} \hat{a}_L^{(in)} \rangle + \cdots,
\end{aligned}
\tag{A3}
$$

$$
\begin{aligned}
\langle \hat{a}_R^{(out)\dagger} \hat{a}_R^{(out)} \rangle &= |S_{21}|^2 \langle \hat{a}_L^{(in)\dagger} \hat{a}_L^{(in)} \rangle + |S_{22}|^2 \langle \hat{a}_R^{(in)\dagger} \hat{a}_R^{(in)} \rangle \\
&\quad + S_{21}^* S_{22} \langle \hat{a}_L^{(in)\dagger} \hat{a}_R^{(in)} \rangle \\
&\quad + S_{21} S_{22}^* \langle \hat{a}_R^{(in)\dagger} \hat{a}_L^{(in)} \rangle + \cdots.
\end{aligned}
\tag{A4}
$$

Here the matrix components $S_{11}$ and $S_{22}$ ($S_{12}$ and $S_{21}$) represent the total amplitude transmission (reflection) coefficients of the network. Under the reciprocity principle, we set $S_{11} = S_{22} \equiv t$. All contributions in (A3) and (A4), containing amplitudes $\hat{b}_m^{(in)}$ and noise operators $\hat{f}$, are denoted as "$\cdots$", and they average to zero since the corresponding modes are in a vacuum state.

In order to fulfill (A2), a combination of a quantum state of light and optical response of the structure should be matched. From now on, we consider the coupling of a single photon coherently distributed between two counterpropagating modes. The path-entangled wave function of the photon is

$$
|\Psi\rangle_{ph} = \alpha |1\rangle_L |0\rangle_R + \beta |0\rangle_L |1\rangle_R,
\tag{A5}
$$

where $\alpha$ and $\beta$ ($|\alpha|^2 + |\beta|^2 = 1$) are probability amplitudes of the photon to propagate from the left (term $|1\rangle_L |0\rangle_R$) and right (term $|0\rangle_L |1\rangle_R$) sides, Fig. 2 of the main text. By substituting (A5) into (A3) and (A4), we obtain two conditions for deterministic light coupling,

$$
t\alpha + S_{12}\beta = 0, \quad S_{21}\alpha + t\beta = 0.
$$

If $\alpha$ or $\beta$ equals zero, i.e., the photon is coming from the one side only, a trivial solution follows: Transmission and reflection coefficients should be equal to zero. Now, if $\alpha \neq 0$ and $\beta \neq 0$,

$$
S_{12} = -\frac{\alpha}{\beta} t, \quad S_{21} = -\frac{\beta}{\alpha} t,
$$

These relations are simplified if we consider a system with a symmetric optical response,

$$
S_{12} = S_{21} \equiv r.
$$

Taking this into account, the following two conditions should be satisfied in order to deterministically couple a single photon into a multinodal network:

(1) The photon should be equally distributed between counterpropagating modes with opposite or equal phase relation between the wave function components,

$$
|\Psi\rangle_{ph} = \frac{1}{\sqrt{2}} (|1\rangle_L |0\rangle_R \mp |0\rangle_L |1\rangle_R),
\tag{A6}
$$

(2) The network, *as a whole*, should be characterized by optical parameters such that transmission and reflection coefficients satisfy opposite to the (A6) phase relation,

$$
t = \pm r,
\tag{A7}
$$

where equal reflection coefficients from both sides are assumed. Interference of arbitrary photon state of the form

$$
|\Psi\rangle_{ph} = \frac{1}{\sqrt{2}} \left( |1\rangle_L |0\rangle_R - e^{i\varphi} |0\rangle_L |1\rangle_R \right)
$$

on the network characterized by (A7) results in phase-dependent probabilities of the photon transmission:

$$
\langle \hat{a}_L^{(out)\dagger} \hat{a}_L^{(out)} \rangle = \langle \hat{a}_R^{(out)\dagger} \hat{a}_R^{(out)} \rangle = |t|^2 (1 - \cos\varphi),
$$

for $t = +r$ and similar for $t = -r$. Since total photon transmission probability should not exceed unity, $t$ must be limited as

$$
|t| \leqslant \tfrac{1}{2}.
$$

We note that similar properties were derived earlier for a single-layer subwavelength coherent perfect absorber [18]. Here, in contrast, we consider dissipation-free systems (if noise operators are omitted and $S$ matrix is unitary) and a photon is coupled to the multinodal system. We note that the solution does not depend on the dimension of the $S$ matrix (i.e., on the number of nodes) nor the nature of light-matter interaction.

The results obtained in this section are valid for classical optical fields as well. To verify this, one may substitute coherent (classical) input states with complex amplitudes $\alpha$ and $\beta$,

$$
|\Psi\rangle_{ph} = |\alpha\rangle_L |\beta\rangle_R,
$$

in (A3) and (A4) instead of the single-photon wave function (A5). Similar conditions, $\beta = \mp\alpha$ and $t = \pm r$, should be fulfilled in this case.

## APPENDIX B: QUANTUM NETWORK WITH NODES OF A SUBWAVELENGTH THICKNESS

In this Appendix, we consider the special case of QNNs of the subwavelength thickness. Despite its practicality (many practical realizations of QNNs are of a subwavelength thickness), this type of node allows us to clearly present the standing wave argument standing behind our approach. For instance, the standing wave picture simplifies the problem of the creation of the state described by Eq. (1) of the main text: When QNNs of the network are placed at the *antinodes of the standing wave*, all of them "see" the same field (interact with the same optical mode), and photon distribution between the nodes is defined by the mutual relation between optical responses of individual nodes. Thus, establishing conditions for deterministic photon coupling does not require knowledge of the entire $S$ matrix, rather a determination of the optical response of individual nodes that fulfill simpler requirements for transmission and reflection of the whole structure. At the same time, such QN would be transparent for the standing wave of the opposite symmetry (or shifted standing wave), since all the QNNs now are at the *nodes of the standing wave* where the electric field is zero and interaction does not happen.

To be specific, we assume that a single photon interacts with plasmonic structures (layers) as demonstrated in multiple experiments [16,18,19,27,66]. By tailoring the optical properties of a single layer, it is possible to achieve the required optical response [18]:

$$r = -t = -1/2. \tag{B1}$$

Now, let us first consider a binodal (bilayered) structure with $M = 2$. Each layer is characterized by its transmission, $t_1$ and $t_2$, and reflection, $r_1$ and $r_2$, coefficients, and for any thin absorber it is valid [18]:

$$r_1 = t_1 - 1, \quad r_2 = t_2 - 1. \tag{B2}$$

Optical properties of the whole structure are defined as

$$t = \frac{t_1 t_2 e^{ikD}}{1 - r_1 r_2 e^{2ikD}}, \tag{B3}$$

$$r' = r_1 + \frac{r_2 t_1^2 e^{2ikD}}{1 - r_1 r_2 e^{2ikD}}, \tag{B4}$$

$$r'' = r_2 + \frac{r_1 t_2^2 e^{2ikD}}{1 - r_1 r_2 e^{2ikD}}, \tag{B5}$$

where $D$ is the distance between the layers; $t$, $r'$, and $r''$ are the total amplitude transmission and reflection (for illumination from left and right sides) coefficients. Setting $D = 0$ should bring us back to (B2), providing additional relations between the optical properties of the layers, namely,

$$t = 1/2, \; r' = r'' = -1/2. \tag{B6}$$

Therefore, combining (B1)–(B6) we obtain

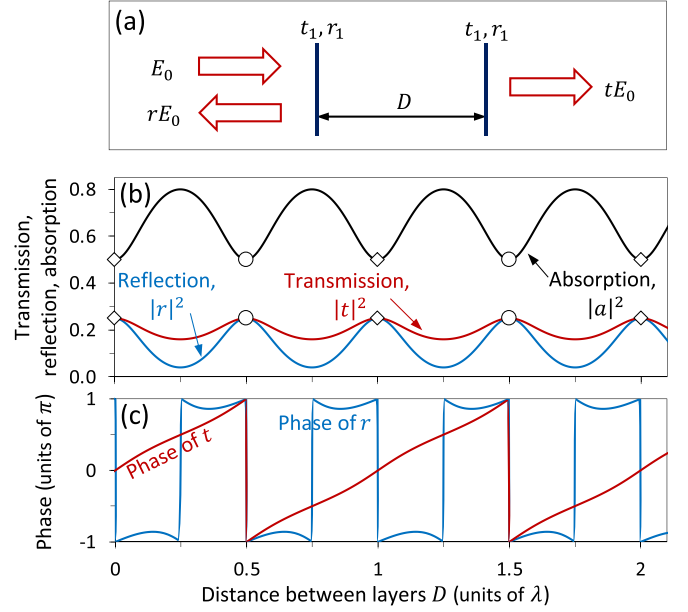$$t_2 = \frac{t_1}{3t_1 - 1}. \tag{B7}$$



FIG. 5. Optical response of a binodal system. (a) Model: two identical layers with $t_1 = 2/3$ and $r_1 = -1/3$ spaced by variable distance $D$. Input monochromatic field with amplitude $E_0$ is partially transmitted ($tE_0$) and partially reflected ($rE_0$). (b) Intensity transmssion $|t|^2$, reflection $|r|^2$, and absorption $|a|^2 = 1 - |t|^2 - |r|^2$ coefficients of the structure as a function of the distance $D$. (c) Phases of transmission and reflection coefficients of the strutcure as a function of the distance $D$. Distance is expressed in units of the wavelength $\lambda$. Diamonds correspond to the regime with $r = -t = -1/2$, while circles correspond to $r = +t = -1/2$.

Letting $t_1$ vary as a free parameter and assuming that the layers are identical, Fig. 5(a), we get

$$t_1 = t_2 = \frac{2}{3} \text{ and } r_1 = r_2 = -1/3. \tag{B8}$$

The optical response of such system is shown in Figs. 5(b) and 5(c) as a function of the distance $D$ between the layers expressed in units of the wavelength $\lambda$. From (B3)–(B5) it follows that relations (B6) and (B7) hold unchanged if the layers are spaced by an integer number of wavelengths, that is, for

$$D = \lambda N, \tag{B9}$$

where $N = 0, 1, 2, \cdots$. As expected, this system absorbs a photon in the symmetric superposition state ($\beta = \alpha = 1/\sqrt{2}$) while it is transparent for the antisymmetric superposition state ($\beta = -\alpha = 1/\sqrt{2}$). Conversely, when the distance between absorbing layers is

$$D = \frac{\lambda}{2}(2N + 1), \tag{B10}$$

the structure is characterized by $r = +t = -1/2$ and has an opposite functionality (it absorbs a photon in the antisymmetric superposition state).

To generalize to the case when the two absorbing layers are separated by a transparent spacer with refractive index $n_{sp}$, (B9) and (B10) should be replaced by

$$D = \frac{\lambda}{2n_{sp}} N, \tag{B11}$$

where (B11) is valid for both types of absorbers. Even though we did not discuss the *S*-matrix components, we still may establish an "empirical" connection between the optical response of individual layers and the resulting quantum state of Eq. (1) of the main text. For instance, the distribution of the absorbed photon between two identical nodes (B8) will be,

obviously, equal. To change the photon distribution between the nodes, one may decrease absorption in one node while increasing it in the other one so that the total response of the system is not changed. Because of the relations (B6) and (B7) only one parameter of the system ($t_1$) defines the resulting state of Eq. (1) of the main text.

[1] A. Acín *et al.*, The quantum technologies roadmap: A European community view, New J. Phys. **20**, 080201 (2018).

[2] H. J. Kimble, The quantum internet, Nature (London) **453**, 1023 (2008).

[3] S. Wehner, D. Elkouss, and R. Hanson, Quantum internet: A vision for the road ahead, Science **362**, eaam9288 (2018).

[4] S. Bose, P. L. Knight, M. B. Plenio, and V. Vedral, Proposal for Teleportation of an Atomic State via Cavity Decay, Phys. Rev. Lett. **83**, 5158 (1999).

[5] C. Cabrillo, J. I. Cirac, P. García-Fernández, and P. Zoller, Creation of entangled states of distant atoms by interference, Phys. Rev. A **59**, 1025 (1999).

[6] J. Volz, M. Weber, D. Schlenk, W. Rosenfeld, J. Vrana, K. Saucke, C. Kurtsiefer, and H. Weinfurter, Observation of Entanglement of a Single Photon with a Trapped Atom, Phys. Rev. Lett. **96**, 030404 (2006).

[7] W. B. Gao, P. Fallahi, E. Togan, J. Miguel-Sanchez, and A. Imamoglu, Observation of entanglement between a quantum dot spin and a single photon, Nature (London) **491**, 426 (2012).

[8] M. Żukowski, A. Zeilinger, M. A. Horne, and A. K. Ekert, "Event-ready-detectors" Bell Experiment via Entanglement Swapping, Phys. Rev. Lett. **71**, 4287 (1993).

[9] J. Hofmann, M. Krug, N. Ortegel, L. Gérard, M. Weber, W. Rosenfeld, and H. Weinfurter, Heralded entanglement between widely separated atoms, Science **337**, 72 (2012).

[10] Y. Zhang, F. S. Roux, T. Konrad, M. Agnew, J. Leach, and A. Forbes, Engineering two-photon high-dimensional states through quantum interference, Sci. Adv. **2**, e1501165 (2016).

[11] B. Jing *et al.*, Entanglement of three quantum memories via interference of three single photons, Nat. Photonics **13**, 210 (2019).

[12] M. Pompili *et al.*, Realization of a multinode quantum network of remote solid-state qubits, Science **372**, 259 (2021).

[13] K. S. Choi, H. Deng, J. Laurat, and H. J. Kimble, Mapping photonic entanglement into and out of a quantum memory, Nature (London) **452**, 67 (2008).

[14] I. Usmani, C. Clausen, F. Bussières, N. Sangouard, M. Afzelius, and N. Gisin, Heralded quantum entanglement between two crystals, Nat. Photonics **6**, 234 (2012).

[15] Y. Wang, J. Li, S. Zhang, K. Su, Y. Zhou, K. Liao, S. Du, H. Yan, and S.-L. Zhu, Efficient quantum memory for single-photon polarization qubits, Nat. Photonics **13**, 346 (2019).

[16] M. S. Tame, K. R. McEnery, Ş. K. Özdemir, J. Lee, S. A. Maier, and M. S. Kim, Quantum plasmonics, Nat. Phys. **9**, 329 (2013).

[17] A. N. Vetlugin, Coherent perfect absorption of quantum light, Phys. Rev. A **104**, 013716 (2021).

[18] T. Roger *et al.*, Coherent perfect absorption in deeply subwavelength films in the single-photon regime, Nat. Commun. **6**, 7031 (2015).

[19] A. N. Vetlugin, R. Guo, A. Xomalis, S. Yanikgonul, G. Adamo, C. Soci, and N. I. Zheludev, Coherent perfect absorption of single photons in a fiber network, Appl. Phys. Lett. **115**, 191101 (2019).

[20] S. M. Barnett, J. Jeffers, A. Gatti, and R. Loudon, Quantum optics of lossy beam splitters, Phys. Rev. A **57**, 2134 (1998).

[21] M. Sabooni, Q. Li, S. Kröll, and L. Rippe, Efficient Quantum Memory Using a Weakly Absorbing Sample, Phys. Rev. Lett. **110**, 133604 (2013).

[22] L. Wang, J. Hu, J. Du, and K. Di, Broadband coherent perfect absorption by cavity coupled to three-level atoms in linear and nonlinear regimes, New J. Phys. **23**, 123040 (2021).

[23] L. M. Duan, M. D. Lukin, J. I. Cirac, and P. Zoller, Long-distance quantum communication with atomic ensembles and linear optics, Nature (London) **414**, 413 (2001).

[24] M. A. Nielsen, Optical Quantum Computation Using Cluster States, Phys. Rev. Lett. **93**, 040503 (2004).

[25] M. Gu, C. Weedbrook, N. C. Menicucci, T. C. Ralph, and P. van Loock, Quantum computing with continuous-variable clusters, Phys. Rev. A **79**, 062318 (2009).

[26] G. Chiribella, G. M. D'Ariano, and P. Perinotti, Quantum Circuit Architecture, Phys. Rev. Lett. **101**, 060401 (2008).

[27] B. Vest, M. C. Dheur, E. Devaux, A. Baron, E. Rousseau, J. P. Hugonin, J. J. Greffet, G. Messin, and F. Marquier, Anti-coalescence of bosons on a lossy beam splitter, Science **356**, 1373 (2017).

[28] A. Manukhova, A. Rakhubovsky, and R. Filip, Atom-mechanical Hong-Ou-Mandel interference, Quantum **6**, 686 (2022).

[29] M. A. Seidler, X. J. Yeo, A. Cerè, and C. Kurtsiefer, Spectral Compression of Narrowband Single Photons with a Resonant Cavity, Phys. Rev. Lett. **125**, 183603 (2020).

[30] J. M. Arrazola *et al.*, Quantum circuits with many photons on a programmable nanophotonic chip, Nature (London) **591**, 54 (2021).

[31] J. Wang *et al.*, Multidimensional quantum entanglement with large-scale integrated optics, Science **360**, 285 (2018).

[32] N. Sangouard, C. Simon, H. de Riedmatten, and N. Gisin, Quantum repeaters based on atomic ensembles and linear optics, Rev. Mod. Phys. **83**, 33 (2011).

[33] A. N. Vetlugin and I. V. Sokolov, Multivariate quantum memory as controllable delayed multi-port beamsplitter, Europhys. Lett. **113**, 64005 (2016).

[34] J. L. Everett, P. Vernaz-Gris, G. T. Campbell, A. D. Tranter, K. V. Paul, A. C. Leung, P. K. Lam, and B. C. Buchler, Time-reversed and coherently enhanced memory: A single-mode quantum atom-optic memory without a cavity, Phys. Rev. A **98**, 063846 (2018).

[35] M. Cao, F. Hoffet, S. Qiu, A. S. Sheremet, and J. Laurat, Efficient reversible entanglement transfer between light and quantum memories, Optica **7**, 1440 (2020).

[36] N. I. Masalaeva, A. N. Vetlugin, and I. V. Sokolov, Cavity-assisted squeezing and entanglement: Non-adiabatic effects and optimal cavity-atomic ensemble matching, Phys. Scr. **95**, 034009 (2020).

[37] N. V. Corzo, B. Gouraud, A. Chandra, A. Goban, A. S. Sheremet, D. V. Kupriyanov, and J. Laurat, Large Bragg Reflection from One-Dimensional Chains of Trapped Atoms Near a Nanoscale Waveguide, Phys. Rev. Lett. **117**, 133603 (2016).

[38] H. L. Sørensen, J. B. Béguin, K. W. Kluge, I. Iakoupov, A. S. Sørensen, J. H. Müller, E. S. Polzik, and J. Appel, Coherent Backscattering of Light Off One-Dimensional Atomic Strings, Phys. Rev. Lett. **117**, 133604 (2016).

[39] J. D. Siverns, S. Weidt, K. Lake, B. Lekitsch, M. D. Hughes, and W. K. Hensinger, Optimization of two-dimensional ion trap arrays for quantum simulation, New J. Phys. **14**, 085009 (2012).

[40] A. Nandi, H. An, and M. Hosseini, Coherent atomic mirror formed by randomly distributed ions inside a crystal, Opt. Lett. **46**, 1880 (2021).

[41] H. Bernien *et al.*, Probing many-body dynamics on a 51-atom quantum simulator, Nature (London) **551**, 579 (2017).

[42] K. Wright *et al.*, Benchmarking an 11-qubit quantum computer, Nat. Commun. **10**, 5464 (2019).

[43] Y. Nam *et al.*, Ground-state energy estimation of the water molecule on a trapped-ion quantum computer, npj Quantum Inf. **6**, 33 (2020).

[44] M. Mielenz *et al.*, Arrays of individually controlled ions suitable for two-dimensional quantum simulations, Nat. Commun. **7**, ncomms11839 (2016).

[45] I. Buluta and F. Nori, Quantum simulators, Science **326**, 108 (2009).

[46] A. V. Poshakinskiy, J. Zhong, Y. Ke, N. A. Olekhno, C. Lee, Y. S. Kivshar, and A. N. Poddubny, Quantum Hall phases emerging from atom–photon interactions, npj Quantum Inf. **7**, 34 (2021).

[47] D. G. Baranov, A. Krasnok, T. Shegai, A. Alu, and Y. D. Chong, Coherent perfect absorbers: Linear control of light with light, Nat. Rev. Mater. **2**, 17064 (2017).

[48] Y. D. Chong, L. Ge, H. Cao, and A. D. Stone, Coherent Perfect Absorbers: Time-Reversed Lasers, Phys. Rev. Lett. **105**, 053901 (2010).

[49] W. Wan, Y. D. Chong, L. Ge, H. Noh, A. D. Stone, and H. Cao, Time-reversed lasing and interferometric control of absorption, Science **331**, 889 (2011).

[50] J. F. Zhang, K. F. MacDonald, and N. I. Zheludev, Controlling light-with-light without nonlinearity, Light Sci. Appl. **1**, e18 (2012).

[51] D. G. Baranov, A. Krasnok, and A. Alù, Coherent virtual absorption based on complex zero excitation for ideal light capturing, Optica **4**, 1457 (2017).

[52] S. Huang and G. S. Agarwal, Coherent perfect absorption of path entangled single photons, Opt. Express **22**, 20936 (2014).

[53] T. Roger, S. Restuccia, A. Lyons, D. Giovannini, J. Romero, J. Jeffers, M. Padgett, and D. Faccio, Coherent Absorption of N00N States, Phys. Rev. Lett. **117**, 023601 (2016).

[54] C. Altuzarra, S. Vezzoli, J. Valente, W. B. Gao, C. Soci, D. Faccio, and C. Couteau, Coherent perfect absorption in metamaterials with entangled photons, ACS Photonics **4**, 2124 (2017).

[55] A. Ü. C. Hardal and M. Wubs, Quantum coherent absorption of squeezed light, Optica **6**, 181 (2019).

[56] A. Lyons, D. Oren, T. Roger, V. Savinov, J. Valente, S. Vezzoli, N. I. Zheludev, M. Segev, and D. Faccio, Coherent metamaterial absorption of two-photon states with 40% efficiency, Phys. Rev. A **99**, 011801(R) (2019).

[57] A. N. Vetlugin, R. Guo, C. Soci, and N. I. Zheludev, Anti-Hong-Ou-Mandel effect with entangled photons, arXiv:2105.05444 [quant-ph].

[58] O. Hernández and I. Liberal, A generalized approach to quantum interference in lossy *N*-port devices via a singular value decomposition, arXiv:2108.12160 [physics.optics].

[59] A. Z. Goldberg and K. Heshami, How squeezed states both maximize and minimize the same notion of quantumness, Phys. Rev. A **104**, 032425 (2021).

[60] A. N. Vetlugin, C. Soci, and N. I. Zheludev, Modelling quantum photonics on a quantum computer, arXiv:2111.15183 [quant-ph].

[61] N. Tischler, C. Rockstuhl, and K. Słowik, Quantum Optical Realization of Arbitrary Linear Transformations Allowing for Loss and Gain, Phys. Rev. X **8**, 021017 (2018).

[62] A. Xomalis *et al.*, Fibre-optic metadevice for all-optical signal modulation based on coherent absorption, Nat. Commun. **9**, 182 (2018).

[63] B. Chen, R. Bruck, D. Traviss, A. Z. Khokhar, S. Reynolds, D. J. Thomson, G. Z. Mashanovich, G. T. Reed, and O. L. Muskens, Hybrid photon–plasmon coupling and ultrafast control of nanoantennas on a silicon photonic chip, Nano Lett. **18**, 610 (2018).

[64] S. Yanikgonul, R. Guo, A. Xomalis, A. N. Vetlugin, G. Adamo, C. Soci, and N. I. Zheludev, Phase stabilization of a coherent fiber network by single-photon counting, Opt. Lett. **45**, 2740 (2020).

[65] https://doi.org/10.21979/N9/7EWOX1.

[66] E. Altewischer, M. P. van Exter, and J. P. Woerdman, Plasmon-assisted transmission of entangled photons, Nature (London) **418**, 304 (2002).